Functional intra-operative guidance of the cavernous nerve network using near-infrared cyanine voltage-sensitive dye imaging: relevance for nerve-sparing radical prostatectomy

Jeeun Kang[1,*], Hanh N. D. Le[2,*], Serkan Karakus[3], Adarsha P. Malla[4], Maged M. Harraz[4], Jin U. Kang[2], Arthur L. Burnett[3], Emad M. Boctor[1,]**

[1] Russell H. Morgan Department of Radiology and Radiological Science, Johns Hopkins Medical Institutions, Baltimore, MD 21231, United States;

[2] Department of Electrical and Computer Engineering, Whiting School of Engineering, Johns Hopkins University, Baltimore, MD 21218, United States;

[3] The James Buchanan Brady Urological Institute, Johns Hopkins Medical Institutions, Baltimore, MD 21287, United States;

[4] Solomon H. Snyder Department of Neuroscience, Johns Hopkins Medical Institutions, Baltimore, MD 21205, United States.

* These authors were equally contributed.

**eboctor1@jhmi.edu

Abstract

Despite current progress achieved in the surgical technique of radical prostatectomy, post-operative complications such as erectile dysfunction and urinary incontinence persist at high incidence rates. In this paper, we present a functional intra-operative guidance of the cavernous nerve (CN) network for nerve-sparing radical prostatectomy using near-infrared cyanine voltage-sensitive dye (VSD) imaging, which visualizes membrane potential variations in the CN and its branches (CNB) in real time. As a proof-of-concept experiment, we demonstrated a functioning complex nerve network in response to electrical stimulation of the CN, which was clearly differentiated from surrounding tissues in an *in vivo* rat prostate model. Stimulation of erection was confirmed by correlative intracavernosal pressure (ICP) monitoring. Within 10 min we performed trans-fascial staining of the CN by direct VSD administration. Our findings suggest the applicability of VSD imaging for nerve-sparing radical prostatectomy.

Introduction

Despite the remarkable evolution in radical prostatectomy (RP) from the radical perineal prostatectomy reported by Young to the nerve-sparing radical retropubic prostatectomy (RRP) described by Walsh[1-3], post-operative complications such as erectile dysfunction, in particular, persist, partly due to surgical damage to erection producing cavernous nerves (CN) resulting from this prostate cancer treatment. Because of the proximity of the CN to the prostate gland, at an average distance of 2.8 mm, these nerves are at risk for injury during the surgical procedure. Also, it is still unknown to what extent CN branches (CNB), surrounding the prostate with a spray-like distribution[4], contribute to erectile function. The CNB are contained within the periprostatic and levator fascias, part of which require dissection to access the prostate surgically. The individual CN are a few hundreds of micrometers in diameter and the CNB are even thinner, making it difficult to predict the exact locations and paths of these nerves, as they vary from one patient to another.[5] Despite the innovation of laparoscopic/robotic RP[6], post-operative erectile function recovery outcomes have not necessarily improved over time with only approximately 70% fully restored potency rates at 12 months after

surgery.[7] Irrespective of surgical approach, RP demands an improved understanding of the anatomical features of the surgery, particularly with respect to the functional anatomy of the CN network for its maximal preservation.[8]

Fluorescence (FL) imaging has been advanced as a significant tool in the field of intra-operative imaging. Intriguing commercial solutions have been recently introduced such as the FireFly™ (Intuitive Surgical Inc., United States) and the FLARE™ systems (Curadel ResVet Imaging, LLC., United States)[10,11], and several exogenous fluorophores targeted to specific tissue types have also been proposed.[12-14] Enthusiasm for FL imaging in academia and industry originated from its wide field-of-view (FOV) directly superimposable on the surgeon's visual field, making it amenable to conventional surgeries including RP. Most of the current nerve-specific fluorophores demonstrate nerve networks with high affinity, but this mechanism will only yield stationary locations of nerves, rather than establish their electrophysiological activity based on erection functionality.[13,15] Furthermore, most of these nerve-specific fluorophores only provide a superficial imaging depth, because they have peak absorption and emission wavelengths at the visible wavelength range (400-650nm). Although several research presentations have recently suggested the applicability of infrared dyes to intra-operative nerve localization, they are still based on a nerve-specific affinity mechanism, rather than on the functional resolution of a patient's erectile function.[16,17] Also, nerve labelling with this affinity-based mechanism takes a long time, from a few hours to days. A direct administration method for near-infrared dye was recently proposed to address this problem, but it is still based on the affinity-based mechanism.[14]

Recently, we proposed the novel mechanism of cyanine voltage-sensitive dye (VSD) imaging, which redistributes the concentration of dyes according to cell membrane potential, displaying functional contrast that corresponds to electrophysiological events in biological tissue.[18,19] In detail, the cyanine dye with positively-charged chemical structure (e.g., IR780 perchlorate) is attracted into the cell membranes when the neuronal cells are in their polarized resting state (i.e., -90mV).[20] The increase of VSD concentration inside the cell membrane triggers their aggregation, leading to FL quenching that dissipates the absorbed light energy in the form of thermal energy. Conversely, when the neuronal cells are in their depolarized state, the VSD aggregate is disassembled and dispersed back into the intra-/extra-cellular spaces. This redistribution restores FL emission. This functional contrast change is activated in sequences of neuronal depolarization and can be quantified by FL imaging at its near-infrared peak absorption and emission wavelengths at 790nm and 820nm, respectively (Figure S1), which is beneficial for deep FL imaging. From the commercially-available VSD compound (IR780 perchlorate), 69.69% of fractional contrast in FL emission is obtained with 6-μM VSD concentration when depolarized from -120mV of membrane potential.[19] Our team also presented the feasibility of transcranial FL VSD neuroimaging using this VSD compound.[21]

In this paper, we present an *in vivo* proof-of-concept of intra-operative FL imaging guidance using the near-infrared cyanine VSD responses evoked by penile erection stimulation using a rodent animal model. Our major hypothesis is that the FL quenching-based VSD mechanism presents the functional contrast of the periprostatic erectogenic nerve network that reacts to an electrical stimulus in real-time. The temporal response time for VSD redistribution occurs at a sub-second scale,[18] suggesting that the real-time calibration for a surgeon's performance will be enabled during RP. Also, we applied direct VSD administration to the rat periprostatic nerves situated within intact levator and periprostatic fascia layers. The staining time is designed to be within 10 min so that it would not delay or hamper the current standard RP protocol.

Results

Near-infrared FL imaging of electrically-stimulated erectile function. The FL imaging fiberscope was designed to provide similar endoscopic view as in a clinical flexible fiberscope. At the distal end of the fiberscope is a customized optical assembly to focus high angle beams (70-degree field of view) from the object into the fiber core body. The focused image at the distal fiber end is then relayed multiple times to the proximal fiber end through total internal reflectance. The customized optical

assembly with 1.5-mm lens diameter was optimized using Optics Studio 15 SP1 (Zemax, Kirkland, Washington, USA), fabricated, and housed in front of the fiber relay body. The simulation layout, spot diagram, and modulated transfer function (MTF) of the optical assembly is shown in Figure S2. The resultant numerical aperture (NA) of the fiberscope was approximately 0.398. The fiber relay body (not shown in Figure S2) is a fiber bundle with 50,000 cores in 1,100-µm diameter at 4.5-µm pixel center-to-center spacing (FIGH-50-1100N, Fujikura Image Fiber Bundles, Myriad Fiber Imaging, MA). The relayed image near the proximal fiber end is focused to a scientific CMOS sensor (Hamamatsu ORCA-Flash4.0) using a 10X microscope objective lens (Bausch & Lomb Objective, Microscope Central, PA). The FL signal from the collected relayed image is filtered to the sensor with a long pass hard-coated dielectric coating filter at cut-on wavelength at 800 nm (FELH0800, Thorlabs, New Jersey, USA).

For the laser illumination, a 100-mW diode laser with central wavelength at 785 nm (FWHM 3 nm) equipped with a variable beam expansion lens is mounted on a separated arm to illuminate the sample. The position of laser illumination was aimed to cover a rat prostate region with illumination circle of 1 cm. The overall system configuration with the imaging fiber, the laser source, the nerve excitation and ICP monitoring is shown in Figure 1.

The frame rate of the CMOS camera was approximately 2fps with 500 msec of exposure time. For the laser illumination, a 100mW laser diode was used in front to illuminate an area of about 1cm in diameter. The position of laser illumination was aimed to cover a rat prostate region before starting the experiments. Please refer the supplementary information for detailed specifications of the imaging system (Figure S3). The bipolar electrical stimulation module was connected to the right CN to induce the controlled CN stimulation upon the electrical pulse excitation: 4-volt square-wave pulse for 5 msec at 16Hz.[22] At the same time, intracavernosal pressure (ICP) was measured to quantify the blood flow into penis evoked by neurovascular coupling from the stimulation. The FL imaging was conducted for 5 min after the VSD staining procedures onto the rat prostate surface, and stimulation was performed for 1 min (1 min – 2 min) during the image recording (Figure 2a).

Intracavernosal pressure monitoring. ICP monitoring validated the erectile function induced by CN electrical stimulation.[23] Experiments were conducted for rats with and without VSD staining procedures. Figure 2b shows the trace of ICP value change over time during an *in vivo* experiment. The significant ICP increase was detected from the rat with VSD staining when electrical stimulation is induced. Maximal and basal ICP values in VSD group (n=3) were 70.62±15.18mmHg and 15.14±2.93mmHg, respectively. On the other hand, the control rat group (n=3) presented comparable level of ICP trace with maximal and basal ICP values at 69.89±1.92mmHg and 9.22±3.10mmHg, respectively. This indicates preserved erectile function in rat model despite effects of the surgical procedures and direct VSD administration at given concentrations, staining durations, and flushing procedures, etc. The stimulated erectile response in VSD group was also validated with the observations of tumescence and detumescence as shown in Figure 2c and Movie 1.

Intra-operative nerve localization. Figure 3a presents the white-light and FL images obtained from the given FOV on the rat prostate. The right CN (RCN) branching from the major pelvic ganglion (MPG) was differentiable to the naked eye during the surgery in white-light image, and clear FL emission was detected from the entire prostate surface after performing direct VSD administration and flushing out procedures. This manner confirmed the successful binding of VSD within tissues adjacent to the prostate. Figure 3b shows the time-averaged evolutions of fractional FL intensity change (F/F_0) at each image pixel in pre-stimulation, stimulation, and post-stimulation phases from the reference frame averaged for 0 – 0.5 min duration (across 60 frames). The stimulation phase revealed respectively up to 10.56±4.14% and 7.04±4.77 of F/F_0 at the CN and CNB structures with photo-bleaching correction (Figure S4). These results may represent the chain reaction of the nerve network from the CN to CNB with different nerve areas under stimulation. The real-time video is reconstructed in Movie 2. The slight motion in the region-of-interest (ROI) was generated conceivably by the instantaneous blood volume change as a product of electrical stimulation, but it was not significant in our validation study (Figure S5). The normalized cross-correlation coefficient was calculated from the 4×4-mm^2 region-of-interest (ROI) indicated by the dotted square in Figure 3b. Note that this ROI was selected as it yielded the highest F/F_0 from the prostate surface. From this, the worst correlation coefficient was at

0.979 during the stimulation and post-stimulation phase. This confirms the fractional FL contrast in the ROI was not generated by any structural change over time. In addition, we made a counter-hypothesis that the mean FL intensity in the ROI should be constant regardless of stimulation if the contrast was adversely caused by motion artifacts. However, the global FL intensity in the ROI was increased in the stimulation phase and restored back to basal level in the post-stimulation phase. This manner also confirmed that the fractional contrast was contributed by the VSD redistribution mechanism.

Histopathological validation of direct VSD administration. The direct VSD staining procedures were validated to localize rat nerves layered within the periprostatic and levator fascias. Frozen-sectioning and histopathological analysis were performed to demonstrate the penetration of VSD into the CN network in line with the direct administration protocol used. Figure 4 presents the white-light and FL microscopic images obtained from prostate slices, showing sufficient VSD staining depth into nerves interposed between the prostate gland and levator fascia whose thickness is a few hundred µm. The clear round cross-sections of nerve branches were successfully differentiated.

Discussion

The prostate is understood to be the leading organ for new cancer cases and resulting deaths for males in the United States, (180,890, 21% in total cancer diagnosis), according to a 2016 estimate by Siegel, *et al.*[24] Although survival rates have been improved by RP for patients with early-detected prostate cancer, a challenging assignment remains to prevent post-operative erectile dysfunction and/or urinary incontinence, which significantly impact quality of life. To address this concern, surgical guidance technology via integrated medical imaging modalities is offered as a revolutionary direction, as summarized in Table 1.[5,10,11] In general, each of the intra-operative guiding modalities aims to provide clear information on the tumor or the periprostatic nerves to a surgeon. They are categorized into two primary approaches. One approach of pre-operative imaging and real-time registration serves to utilize high contrast imaging in wide imaging volume available with pre-operative tomographic imaging modalities, such as positron emission tomography (PET), computed tomography (CT) and magnetic resonance imaging (MRI). However, each modality has its own disadvantages: limited spatial resolution not optimal for CNB imaging (PET); ionizing radiation on a patient (PET, CT); no functional contrast describing the relevant CN (PET, MRI, CT); high cost (PET, CT, MRI). In addition, even though a surgical guidance device should be well implemented in the operating room, it necessitates a sophisticated tracker on a patient. This may hamper either an operation or the image registration to a surgeon's view because variations in environments may affect the registration performance (e.g., movements of multiple surgeons and equipment nearby a patient).[25-27] An alternative approach applies intra-operative real-time imaging and display technologies, and several have been proposed operating mostly as area- and cost-effective acoustic and optical imaging modalities such as ultrasound imaging (US), optical coherence tomography (OCT), coherent anti-stroke Raman spectroscopy (CARS), confocal microscopy (CFM), multi-photon microscopy (MPM), and FL imaging. Since real-time feedback is available with these modalities, a surgeon's performance can be instantly calibrated. However, they also suffer from limitations such as: limited spatial resolution and low contrast (US); no functional contrast describing the relevant CN (US, OCT); and superficial imaging depth (CARS, CFM, MPM). However, near-infrared FL imaging has been highlighted to offer an in intra-operative imaging field with advantages in compact system volume, wide FOV and relatively deep imaging depth (~few mm).

In this paper, we present an *in vivo* proof-of-concept of a novel functional nerve-guidance method that may easily be amenable to the current standard RP protocol. The functional FL imaging of the VSD-stained rat prostate presented the complex nerve network (CN + CNB) distinct from the surrounding tissues only when CN electrical stimulation is induced (Figure 3). This result was enabled by our FL quenching yield changing VSD mechanism, which reflects depolarization events happening in the relevant nerve network in response to stimulation applied to the CN. Successful direct VSD administration to nerves was confirmed by histopathological analysis (Figure 4). The 10-min duration for VSD staining is brief and should not hamper RP surgical procedures.

We plan a number of follow-up studies to further advance the proposed intra-operative nerve-sparing guidance method. The characteristics of VSD may be further improved to produce a higher fractional contrast change in FL emission between polarized and depolarized states, while providing a higher absorption coefficient at near-infrared range for better imaging sensitivity. Also, exploiting the positively-charged electrochemical property of VSD may enhance staining efficiency based on increased responsiveness to the membrane potential variation in the CN nerve network. Furthermore, the temporality of VSD redistribution may be an important parameter to better understand. The results shown in Figure S2 suggest the different temporal features of VSD redistribution in membrane depolarization and repolarization events during transitions in stimulation and post-stimulation phases, respectively. Therefore, further analysis of VSD characteristics will enhance perspectives for optimizing real-time nerve functionality quantification in real time. We will also address toxicity concerns of the proposed cyanine VSD. Our team is optimistic of its safety because as it is composed by a chromophore identical to that present in FDA-approved indocyanine green (ICG). On the proposed method, the direct tissue contact of VSD solution will be limited to the prostatic region for 10 min at most, and the amount perfused into a patient's blood stream will be negligible. For these reasons, the possibility of chemical toxicity effects for a patient's body is likely low. We already presented that the direct VSD administration did not exert any adverse objective or subjective effects on erectile function (Figure 2b and 2c). We will validate this observation in future investigations.

The detailed methodology of the direct VSD staining protocol should be further improved to represent a more quantitative measure of membrane potential variations. In the *in vivo* study shown in this paper, the majority of the VSD solution ran down from the prostate surface based on the angled position, and only the top part of the prostate accumulated the VSD solution. This condition possibly led to the results in Figure 3b defining the highest F/F_0 at the center of the prostatic region. Therefore, optimizing the direct trans-fascia VSD delivery will be pursued in our future studies. A patch-based delivery method may well be investigated to achieve both fast, uniform VSD delivery and easier translation simultaneously.

We are very eager to extend this concept to a multi-modal surgical guidance approach incorporating PA and FL imaging modalities. There have been several extensions into multi-modal imaging applying the above two approaches for intra-operative guidance: MRI + transrectal US[28]; photoacoustic microscopy (PAM) + OCT[29]; PET + FL[30]; US + photoacoustic tomography (PAT) + FL[31,32]. However, no such attempts can achieve enough synergy without a multi-modal VSD indicator for any proposed application. PA imaging is an emerging hybrid imaging modality providing both optical absorptive contrast and acoustic imaging depth, and it also supports versatile imaging scales by microscopic (5 µm of spatial resolution for up to 2 mm-depth) and tomographic imaging configurations (~800 µm of spatial resolution for up to 7-cm depth).[33-35] Also, recently several PA neuroimaging researchers have proposed to quantify membrane potential variations using a genetically-encoded calcium indicator or non-radiative voltage sensor.[22,23] We have also shown the concept of novel functional PA imaging of membrane potential variation *in vivo* using the same cyanine VSD used in this study (i.e., IR780 perchlorate). The study was based on the complementary PA and FL contrast according to the stated VSD redistribution mechanism. When nerves are in the polarized state, the absorbed light energy on VSD aggregates will be more dissipated in the form of thermal energy, which will trigger a thermal expansion of the surrounding thermoelastic medium, e.g., water contents or soft tissue. The acoustic energy can be detected by a clinical ultrasound transducer posed at a transrectal configuration or outside of body. On the other hand, the dissolution of VSD aggregates in the nerve's depolarized state will lower the PA generation efficiency back to its original level. We have already validated the VSD mechanism via controlled lipid vesicle experiments with various membrane potential levels and further presented *in vivo* brain imaging using rat seizure and NMDA infusion models.[19,36] This approach may promise more comprehensive nerve-sparing guidance extended to entire surgical procedures. For example, it may extend to pre-operative planning, intra-operative guidance, and post-operative monitoring of the treatment outcome. Pre-operative applications may delineate nerve distributions before making incisions; intra-operative guidance using reciprocal contrast in PA and FL imaging may maximize sensitivity based on membrane potential; and post-operative monitoring using non-invasive transrectal PA imaging may assess erectile function recovery. We also developed a dual-

modal imaging system using a pulsed Nd:YAG optical parametric oscillator (OPO) laser, which produces FL and PA contrast from the same absorber target. Further investigation will lead to optimized engineering solutions to facilitate its translation into pre-clinical animal studies and, eventually, to human investigations.

Further translational study may advance the concept of CN stimulation. In the clinical management field of erectile dysfunction, electrical nerve stimulation has been used in general due to its simple and intuitive configuration. However, there is the possibility to cause nerve damage from direct physical contact of electrodes on nerve structures, and the erectile function response is inconsistent, indicating low specificity of this proposed method. Moreover, there have been several studies citing the frequent degradation of parallel recording accuracy with electrical activity.[38] Several promising and safer stimulation methods can be used. A continuous-wave infrared subsurface optical stimulation method using infrared wavelengths (i.e., 1,490nm and 1,870nm) was successfully used to induce erection in a rat model comparable to that obtained from electrical stimulation. The non-contact configuration on the CN is advantageous in terms of prevention of any physical damage.[38-40] Also, the impact of non-invasive ultrasound stimulation has recently been highlighted with safe acoustic intensity at a localized region with high spatial selectivity.[41,42] The realization of remote control of erectile function using its deep focusing capability would be enormous to improve the safety for the controlled activation of erection during RP.

In our future translation, a greater number of rodent animals will be included based on an improved experimental setup, and the practical CNB contribution to erectile function will be further studied. The extent of the localized nerve damage induced to CNB with various distances from the primary CN will be assessed, and the area of the damage will be controlled based on various techniques.[37] CN stimulation and ICP measurement protocols will be also applied for quantitative evaluation. This investigation will show the extent to which CNB actually contribute to the erectile function in addition to the primary CN.

A translatable model may be considered for our future validation. Even though the current experimental results are encouraging with the rodent animal model, the guidance specification may not be optimal for other larger animal models or humans – In the rat prostate, the fascia layers surrounding the prostate are very thin at around 100 μm of thickness, whereas the human prostatic fascia is much thicker. In practice, variability in fascia thickness should be further evaluated because this factor may substantially affect the trans-fascial FL imaging and effectiveness of the VSD staining procedure. For this investigation, an *ex vivo* human prostate sample with intact levator and periprostatic fascia layers would be used. VSD droplets with various concentrations would be administered on the sample for various durations, and depths of penetration would be recorded with measurements of local sample thickness. FL imaging would be performed to validate the imaging depth, and the VSD-stained depth could be quantified by subsequent histopathological analysis. This study design would serve to optimize the VSD administration scheme as a function of fascia thickness for further translational *in vivo* study using large animal models (e.g., canine, porcine, etc.) and/or a human trial. In the *in vivo* evaluations, the instant calibration of the direct VSD administration setup may be allowed by a local fascia thickness given by pre-operative tomographic imaging with narrow axial resolution (e.g., US, OCT) or by pre-operative imaging (e.g., CT, MRI).

Methods

Voltage-sensitive dye preparation. The VSD (IR780 perchlorate, 576409, Sigma-Aldrich, Inc., United States) was vortexed in 5% DMSO, 5% Cremophor EL until dissolved, then dilute with 0.9% saline to be 1mM concentration for the proposed *in vivo* experiments. The peak absorbance and FL emission is at 790nm and 820nm, respectively (Figure S1). In our previous study, we presented the FL emission of VSD for varying potassium gradient (i.e., 25, 50, and 100-fold) in a lipid vesicle model. The 6-μM VSD provided up to 69.69% of fractional change in FL emission when the membrane is depolarized from 100-fold of potassium gradient (upper estimate -120 mV).[18,19]

Animal preparation. Adult male Sprague-Dawley rats (325-350g; Charles River Breeding Laboratories, Wilmington, MA, USA) were used. All experiments were approved by the Johns Hopkins University School of Medicine Institutional Animal Care and Use Committee in accordance with the National Institutes of Health Guide for the Care and Use of Laboratory Animals. The rats were anesthetized with intraperitoneal injection of a ketamine (100mg/kg) and xylazine (5mg/kg) mixture. The prostate was exposed via a midline abdominal incision, and CNs and MPGs were located bilaterally posterolateral to the prostate.

***In vivo* experimental protocol.** Figure 2a presents the *in vivo* experimental protocol employed in this study. The 200µl of 1mM VSD in DSMO + Cremophore EL solvent was directly administrated to the rat prostate surface for 10min before starting FL recording. The VSD not bound to the prostate nerve membrane was flushed out for 5min with 2-ml phosphate buffered saline (PBS) solution. For the prostate with VSD administration, FL images were recorded for 5min, and 1min of stimulation was induced from 1min to 3min. There were 1min of pre-stimulation and 3min of post-stimulation phases to track the change of VSD response.

Electrical CN stimulation and intracavernosal pressure monitoring. To monitor ICP, the shaft of the penis was denuded of skin and fascia, and the right crus was punctured with a 23-gauge needle connected via polyethylene-50 tubing to a pressure transducer. For electrically stimulated penile erections, a bipolar electrode attached to a Grass Instruments S48 stimulator (Quincy, MA, USA) was placed on CNs. Stimulation parameters were 4 volts, 16Hz, with square-wave duration of 5 msec for 1 min. ICP was recorded (DI-190, Dataq Instruments, Akron,OH, USA) for 5min; pre-stimulation (1 min), stimulation (1 min), and post-stimulation (3 min). Results were analyzed using the MATLAB program (Mathworks, Natick, MA, USA). At the conclusion of experiments, animals were sacrificed by a lethal intracardiac injection of saturated potassium chloride and prostate, both MPGs, and CNs were collected.

Image acquisition and reconstruction. The FL response recorded from the rat prostate was processed in offline workstation. The FL frames recorded during the first half minute (0 min – 0.5 min) without any electrical stimulation were averaged to form a reference image. Afterwards, the fractional change of FL emission (F/F_0) was calculated at each pixel and at each time point at each time point to derive the VSD response evoked by electrical stimulation.

Frozen-section histopathological analysis of *ex vivo* rat prostate samples. After getting the FL recording, a whole rat prostate was immediately harvested. It was placed in fresh 10% formalin for more than 48 hours with gentle agitation using a conical rotator. Cryoprotection processing was done via a series of sucrose gradients (15%, 20%, 30% for 12-24 hours each). Prostates was frozen-sectioned at 300µm thickness. Slides with tissue sections in ProLong Diamond Anti-face mountant were imaged using the LI-COR Odyssey for FL visualization of VSD perfusion.

Acknowledgements

Financial support was provided by the NIH Brain Initiative under Grant No. R24MH106083-03 and the NIH National Institute of Biomedical Imaging and Bioengineering under Grant No. R01EB01963. Jeeun Kang, Ph.D. is supported by Basic Science Research Program through the National Research Foundation of Korea (NRF) funded by the Ministry of Education (2018R1A6A3A03011551).

Author contributions statement

J. K. designed, delineated, and performed *in vivo* experiments, data processing and analysis, and wrote the first manuscript. H. N. D. L. customized the FL imaging module for intra-operative applications and applied to *in vivo* experiments presented in this manuscript. S. K. prepared the animal model and conducted *in vivo* experiments. A. M. conducted a histopathological validation of the direct VSD administration. E. M. B. conceived the research, and J. U. K., A. L. B., and E. M. B. co-directed the project. All authors edited the manuscript.

Additional information

Competing financial interests: The authors declare no competing financial and/or non-financial interests.

Figures

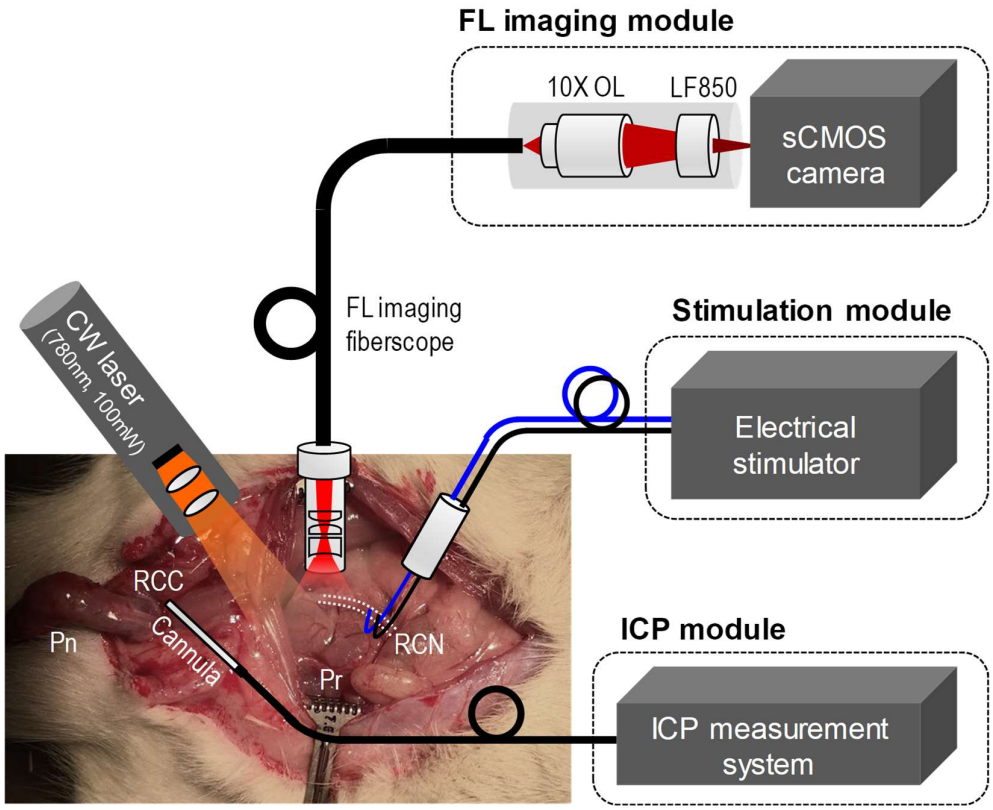

Figure 1. Intra-operative fluorescence (FL) imaging of rat prostatic nerve network *in vivo*. OL, objective lens; LF, emission longpass filter. Pn, penis; RCC, right corpus caverosum; Pr, prostate; RCN, right cavernous nerve; ICP, intracavernosal pressure.

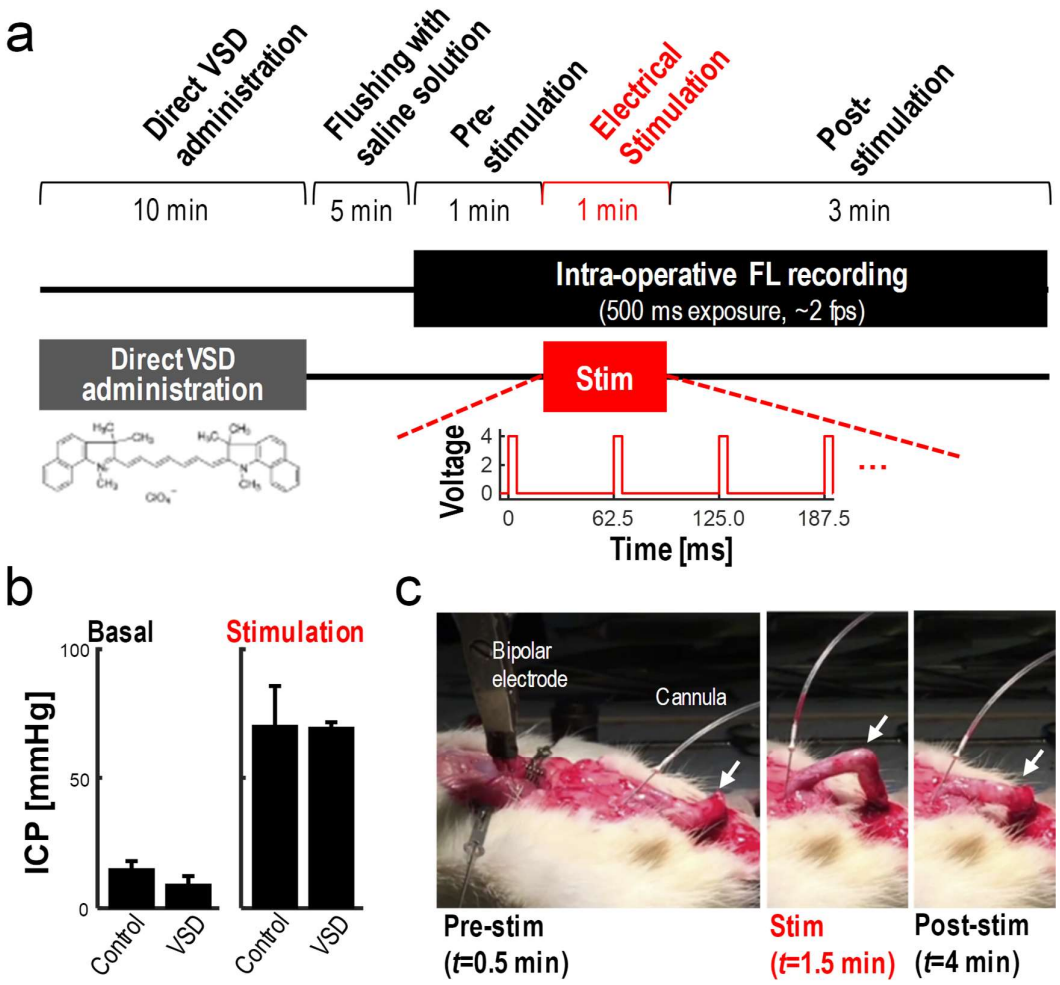

Figure 2. *In vivo* experimental setup for a proof-of-concept of prostatic nerve imaging using near-infrared cyanine VSD: (a) *in vivo* experimental protocol. (b) The validation of an erectile function using intracavernosal pressure (ICP) before and after the electrical stimulation in control and VSD groups. (c) Corresponding observation of erectile function at each experimental phase (Movie 1).

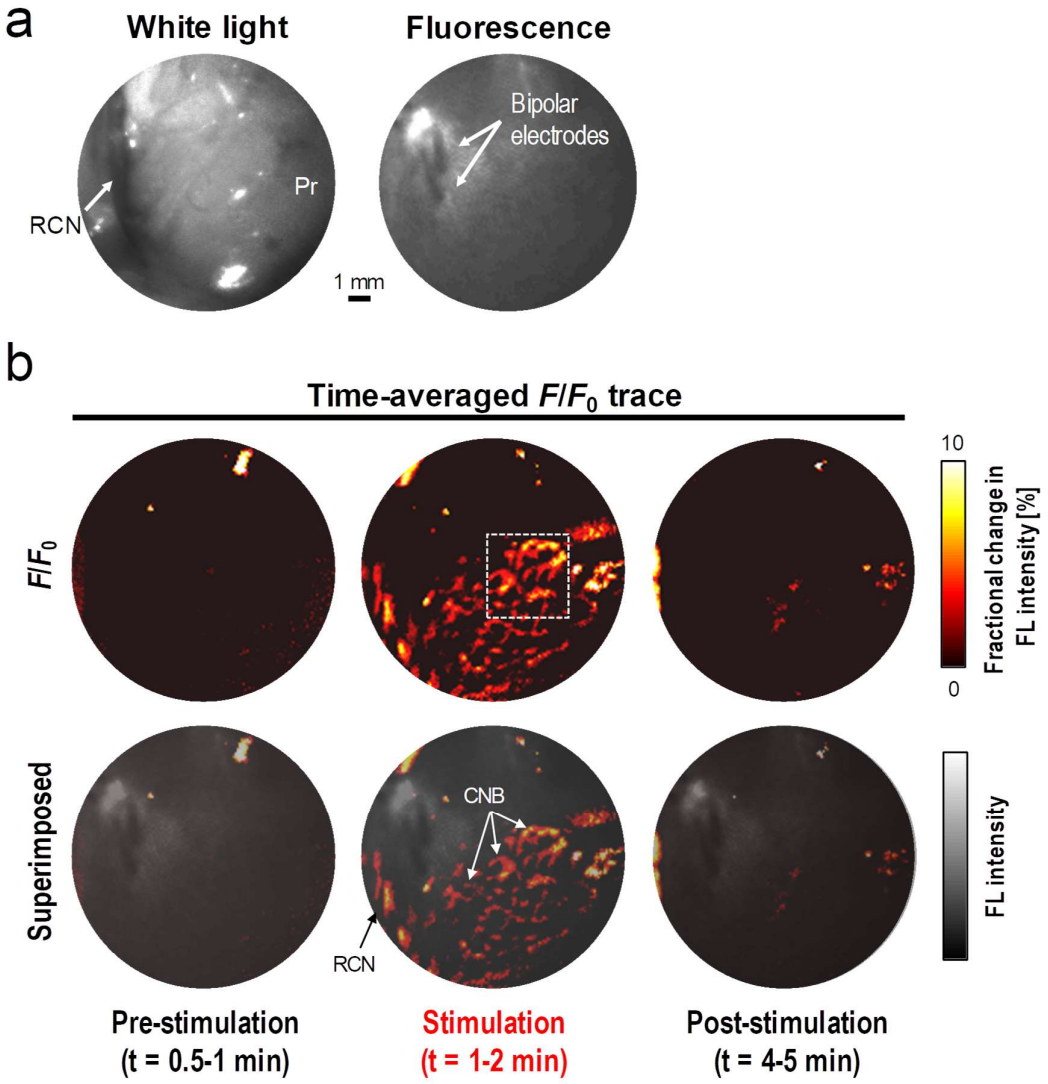

Figure 3. *In vivo* intra-operative nerve localization: (a) white-light and fluorescence (FL) imaging, (b) time-averaged F/F_0 images during stimulation and pre-/post-stimulation phases. RCN, right cavernous nerve; Pr, prostate. The real-time movie of F/F_0 image sequence is available in Movie 2.

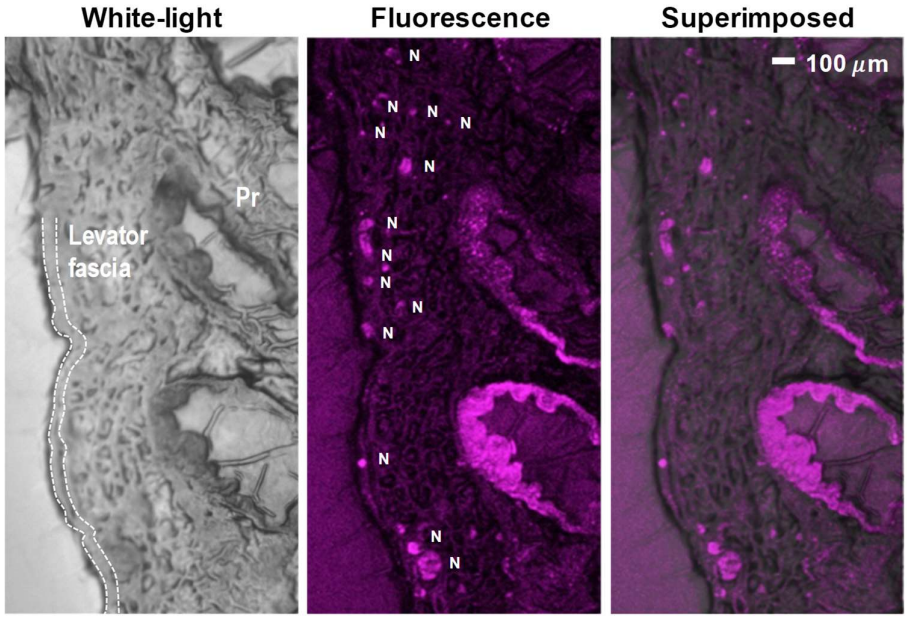

Figure 4. frozen-sectioning histopathological analysis on *ex vivo* rat prostate sample. Dotted line presents the levator fascia covering the prostatic fascia with CNB. White bar indicates 100 μm. Pr, prostate; N, nerve.

Tables

Table 1 Intra-operative imaging modalities for surgical and interventional applications. PET, positron emission tomography; CT, computed tomography; MRI, magnetic resonance imaging; US, ultrasonography; PAT, photoacoustic tomography; PAM, photoacoustic microscopy; OCT, optical tomographic tomography; CARS, coherent anti-strokes Raman spectroscopy; CFM, confocal microscopy; MPM, multi-photon microscopy, FL, fluorescence imaging; DTI, Diffusion tensor imaging.

	Pre-operative imaging and real-time registration			**Intra-operative real-time imaging and display**						
Aims	• Providing real-time and selective contrast information on tumor or nerve systems to surgeons • Using full capacity of high-resolution, high-contrast pre-operative imaging with volumetric wide field-of-view			• Area-, cost-effective solution with a guaranteed registration accuracy between target contrast information on surrounding anatomies • On-site lesion localization before incision		• *In vivo* or *ex vivo* optical biopsy for tissue characterization using molecular contrast				• Targeted contrast agent
Modality	**PET**	**CT**	**MRI**	**US**	**PAT**	**PAM**	**OCT**	**CARS**	**CFM/MPM**	**FL**
Image format	Tomography			Cross-sections and/or volumetric scanning		Raster scanning or *en face* projection from raster-scanned volumetric data				Camera capturing
Spatial resolution	1-2mm	50µm		400µm	800µm	5µm	10µm	~1µm		100µm
Sensing depth	> 30cm			> 20cm	~7cm	~2mm	~2mm	~100µm	~500µm	~100µm – few mm
Throughput	Low			High	Mid		High	Low		High
Cost	High			Low	Not established		Low	Not established		Medium
Toxicity	Yes		No						Yes	
Challenges	• Tricky real-time registration using trackers • Low throughput, high cost • Needs high-end tracker for accurate real-time registration			• Low spatial resolution • Requires contact-mode scanning with acoustic gel coupling		• Suboptimal intra-operative use with superficial sensing depth	• Low throughput • Limited field-of-view		• Long staining time for target labeling (few hrs - days)	
Feasibility on selective imaging of nerve-specific functional information	Metabolism Imaging for injured nerve	-	DTI	-	Quantification of membrane potential variation using calcium indicator or VSD at visible wavelength range (500-600 nm)		-		Quantification of membrane potential variation using organic fluorophores and derivatives at visible wavelength range (400-650 nm)	

References:

1. Young, H. H. The early diagnosis and radical cure of carcinoma of the prostate. Being a study of 40 cases and presentation of a radical operation which was carried out in four cases. (Reprinted from Bull Johns Hopkins University, vol XVI, pg 315-321, 1905). *Journal of Urology* **167,** 939–946 (2002).

2. Walsh, P. C. The Discovery of the Cavernous Nerves and Development of Nerve Sparing Radical Retropubic Prostatectomy. *Journal of Urology* **177,** 1632–1635 (2007).

3. Walsh, P. C. Perfecting nerve-sparing radical prostatectomy: sailing in uncharted waters. *Can J Urol* **15,** 4230–4232 (2008).

4. Park, Y. H., Jeong, C. W. & Lee, S. E. A comprehensive review of neuroanatomy of the prostate. *Prostate International* **1,** 1–7 (2013).

5. Fried, N. M. & Burnett, A. L. Novel methods for mapping the cavernous nerves during radical prostatectomy. *Nat Rev Urol* **12,** 451–460 (2015).

6. Magheli, A. *et al.* Comparison of surgical technique (Open vs. Laparoscopic) on pathological and long term functional outcomes following radical prostatectomy. *BMC Urology 2014 14:1* **14,** 1 (2014).

7. Nielsen, M. E., Schaeffer, E. M., Marschke, P. & Walsh, P. C. High Anterior Release of the Levator Fascia Improves Sexual Function Following Open Radical Retropubic Prostatectomy. *Journal of Urology* **180,** 2557–2564 (2008).

8. Binder, J. & Kramer, W. Robotically-assisted laparoscopic radical prostatectomy. *BJU Int.* **87,** 408–410 (2001).

9. Hu, J. C., Gu, X., Lipsitz, S. R., Barry, M. J. & D'Amico, A. V. Comparative effectiveness of minimally invasive vs open radical prostatectomy. *JAMA* (2009).

10. Manny, T. B., Patel, M. & Hemal, A. K. Fluorescence-enhanced robotic radical prostatectomy using real-time lymphangiography and tissue marking with percutaneous injection of unconjugated indocyanine green: The initial clinical experience in 50 patients. *Eur. Urol.* **65,** 1162–1168 (2014).

11. Troyan, S. L. *et al.* The FLARE™ Intraoperative Near-Infrared Fluorescence Imaging System: A First-in-Human Clinical Trial in Breast Cancer Sentinel Lymph Node Mapping. *Ann Surg Oncol* **16,** 2943–2952 (2009).

12. Park, M. H. *et al.* Prototype Nerve-Specific Near-Infrared Fluorophores. *Theranostics* **4,** 823–833 (2014).

13. Cotero, V. E. *et al.* Improved Intraoperative Visualization of Nerves through a Myelin-Binding Fluorophore and Dual-Mode Laparoscopic Imaging. *PLoS ONE* **10,** e0130276–18 (2015).

14. Barth, C. W. & Gibbs, S. L. Direct Administration of Nerve-Specific Contrast to Improve Nerve Sparing Radical Prostatectomy. *Theranostics* **7,** 573–593 (2017).

15. Gibbs-Strauss, S. L. *et al.* Nerve-Highlighting Fluorescent Contrast Agents for Image-Guided Surgery. *Mol Imaging* **10,** 91–101 (2011).

16. He, K. *et al.* Near-infrared Intraoperative Imaging of Thoracic Sympathetic Nerves: From Preclinical Study to Clinical Trial. *Theranostics* **8,** 304–313 (2017).

17. Wagner, O. J., Louie, B. E., Vallières, E., Aye, R. W. & Farivar, A. S. Near-Infrared Fluorescence Imaging Can Help Identify the Contralateral Phrenic Nerve During Robotic Thymectomy. *ATS* **94,** 622–625 (2012).

18. Zhang, H. K. *et al.* Listening to membrane potential: photoacoustic voltage-sensitive dye recording. *J. Biomed. Opt.* **22,** 045006 (2017).

19. Kang, J. *et al.* Transcranial real-time *in vivo* recording of electrophysiological neural activity in the rodent brain with near-infrared photoacoustic voltage-sensitive dye imaging. *bioRxiv* **202408,** 1–23 (2017).

20. Yang, M. & Brackenbury, W. J. Membrane potential and cancer progression. *Frontiers in Physiology* **4,** 1–15 (2013).

21. Pak, R. W. *et al.* Voltage-sensitive dye delivery through the blood brain barrier using adenosine receptor agonist Regadenoson. *Biomed. Opt. Express* **9,** 3915–3922 (2018).

22. Sezen, S. F. & Burnett, A. L. Intracavernosal pressure monitoring in mice: responses to electrical stimulation of the cavernous nerve and to intracavernosal drug administration. *J. Androl.* **21,** 311–315 (2000).

23. Sezen, S. F. & Burnett, A. L. Intracavernosal pressure monitoring in mice: responses to electrical stimulation of the cavernous nerve and to intracavernosal drug administration. *J. Androl.* **21,** 311–315 (2000).

24. Siegel, R. L., Miller, K. D. & Jemal, A. Cancer statistics, 2016. *CA: A Cancer Journal for Clinicians* **66,** 7–30 (2016).

25. Alam, F., Rahman, S. U., Ullah, S. & Gulati, K. Medical image registration in image guided surgery: Issues, challenges and research opportunities. *Integrative Medicine Research* **38,** 71–89 (2018).

26. Wang, D., Ma, D., Wong, M. L. & Wáng, Y. X. J. Recent advances in surgical planning & navigation for tumor biopsy and resection. *Quant Imaging Med Surg* **5,** 640–648 (2015).

27. Koivukangas, T., Katisko, J. P. & Koivukangas, J. P. Technical accuracy of optical and the electromagnetic tracking systems. *SpringerPlus* **2,** 90–7 (2013).

28. Xu, S. *et al.* Real-time MRI-TRUS fusion for guidance of targeted prostate biopsies. *Computer Aided Surgery* **13,** 255–264 (2010).

29. Lee, D. *et al.* In Vivo Near Infrared Virtual Intraoperative Surgical Photoacoustic Optical Coherence Tomography. *Sci Rep* 1–10 (2016). doi:10.1038/srep35176

30. Zhang, H. *et al.* Dual-Modality Imaging of Prostate Cancer with a Fluorescent and Radiogallium-Labeled Gastrin-Releasing Peptide Receptor Antagonist. *Journal of Nuclear Medicine* **58,** 29–35 (2017).

31. Kang, J. *et al.* A prototype hand-held tri-modal instrument for in vivo ultrasound, photoacoustic, and fluorescence imaging. *Rev. Sci. Instrum.* **86,** 034901 (2015).

32. Kang, J. *et al.* Real-time sentinel lymph node biopsy guidance using combined ultrasound, photoacoustic, fluorescence imaging: in vivo proof-of-principle and validation with nodal obstruction. *Sci Rep* **7,** 45008 (2017).

33. Wang, L. V. & Hu, S. Photoacoustic tomography: in vivo imaging from organelles to organs. *Science* **335,** 1458–1462 (2012).

34. Valluru, K. S., Wilson, K. E. & Willmann, J. K. Photoacoustic Imaging in Oncology: Translational Preclinical and Early Clinical Experience. *Radiology* **280,** 332–349 (2016).

35. Emelianov, S. Y., Li, P. C. & O'Donnell, M. Photoacoustics for molecular imaging and therapy. *Physics today* (2009).

36. Kang, J. *et al.* Transcranial photoacoustic imaging of NMDA-evoked focal circuit dynamics in rat forebrain. *bioRxiv* **308585,** 1–26 (2018).

37. Canguven, O. & Burnett, A. Cavernous nerve injury using rodent animal models. *J Sex Med* **5,** 1776–1785 (2008).

38. Tozburun, S., Lagoda, G. A., Burnett, A. L. & Fried, N. M. Subsurface near-infrared laser stimulation of the periprostatic cavernous nerves. *J. Biophoton.* **5,** 793–800 (2012).

39. Tozburun, S., Cilip, C. M., Lagoda, G. A., Burnett, A. L. & Fried, N. M. Continuous-wave infrared optical nerve stimulation for potential diagnostic applications. *J. Biomed. Opt.* **15,** 055012 (2010).

40. Tozburun, S. *et al.* Continuous-wave Infrared Subsurface Optical Stimulation of the Rat Prostate Cavernous Nerves Using a 1490-nm Diode Laser. *Urology* **82,** 969–973 (2013).

41. Mueller, J., Legon, W., Opitz, A., Sato, T. F. & Tyler, W. J. Transcranial Focused Ultrasound Modulates Intrinsic and Evoked EEG Dynamics. *Brain Stimulation* **7,** 900–908 (2014).

42. Legon, W. *et al.* Transcranial focused ultrasound modulates the activity of primary somatosensory cortex in humans. *Nat. Neurosci.* **17,** 322–329 (2014).